Monitoring of Low Cycle Fatigue Degradation in X6CrNiTi18-10 Austenitic Steel

M. Grosse[1], M. Niffenegger, D. Kalkhof,
Paul Scherrer Institut CH- 5232 Villigen PSI, Switzerland

Abstract

The microstructural changes in the pre-crack stage of low-cycle fatigue damage (LCF) in austenitic piping steels were investigated by neutron and X-ray diffraction. The LCF damage evolution in the metastable austenitic steel causes a deformation-induced phase transformation from austenite to martensite. Thresholds exist for the formation of martensite as a function of accumulated plastic strain. Magnetic stray field and eddy current measurements were chosen to transfer the results of material characterisation to NDT methods. The density and distribution of martensite obtained by neutron diffraction experiments were used to adjust the NDT signals. Both NDT techniques were able to detect the very low amount of martensite in the different fatigued specimens (0.5 - 3.1 vol.-% martensite) with usage factors from 0 up to 1.0.

Keywords: low cycle fatigue, strain-induced martensitic transformation, austenitic steels, non-destructive testing

1. Introduction

The beam window of a pulsed spallation neutron source with liquid metal target is a new challenge for material safety research. Not only neutron and proton embrittlement, liquid metal erosion and corrosion but also thermal fatigue has to be taken into account. This problem is also relevant for continuous spallation sources. Typical beam trip rates of 30 to 50 per day results in loading cycle numbers in the order of magnitude of 10^4 per year. The knowledge about the interaction between fatigue degradation and irradiation hardening and embrittlement in a liquid metal environment is not yet satisfying. Experimental estimation of the fatigue behaviour under irradiation and liquid metal environment are extremely expensive and can only seldom be realised. Online or periodical non-destructive tests of the fatigue state of the target window material can help to ensure the safety of the beam window. In order to develop such test systems experiences of the monitoring of fatigue degradation in comparable materials can be used.

With regard to leaks in pressurised water pipes of nuclear power plants [1], which were caused by thermal fatigue damage, deformation-induced changes in the microstructure of metastable austenitic steel were investigated. It is well known that varying temperatures and thermal stratification in piping of power plants might cause fatigue damage by thermal strains. Such strains promote the phase transition from paramagnetic cubic face centred (fcc) austenite

[1] Corresponding author: Mirco Grosse, Tel.: +41 (0)56 310 2113
Fax: +41 (0)56 310 2199
e-mail: Mirco.Grosse@PSI.Ch

to ferromagnetic cubic body centred (bcc) martensite. This opens the possibility to detect the martensite content by means of magnetometers.
Metallography as well as neutron and X-ray diffraction are primarily intended to identify and quantify martensite formation in the pre-crack stage of low-cycle fatigue damage (LCF) in austenitic piping steels and its influencing parameters. To monitor the pre-crack damage state, the application of magnetic NDT methods based on magnetic stray field and eddy current measurements is investigated.

2. Materials and test conditions

The investigations were performed on hour-glass specimens (according to ASTM E606, Fig. 1). The material under investigation was the titanium stabilised austenitic metastable steel X6CrNiTi18-10, which is widely used for vessels and piping. The chemical composition (in wt.-%) is given in Tab. 1. In order to homogenise the microstructure, the specimens were annealed at 1040 °C (1 h) and afterwards quenched in oil. The total strain controlled fatigue tests were performed with alternating loading and a test frequency of $2\ s^{-1}$ at room temperature. A strain amplitude of ±0.28 % for a gauge length of 25 mm was applied. Due to the shape of the sample the local strain depends on the axial position. As FEM calculations have shown the highest strain amplitude is 0.60 % at the position of the smallest cross section. Different usage factors were realised by well defined cycles of strain loads in series of hour-glass specimens. Tab. 2 gives the cycle number for some investigated specimens and the corresponding usage factor D. The usage factor indicates how much life time is passed for a certain strain amplitude. D is defined to be equal to 1 for specimens, where crack initiation has occurred (5% force drop). Therefore the corresponding cycle numbers vary for specimens with D = 1 due to differences in the damage progression. For specimens without a crack, D is defined as the ratio of the applied cycle number to an averaged cycle number representing crack initiation.

For the metallographic investigations, the specimens were cut in axial direction. After mechanical grinding and polishing, the specimens were etched with Beraha-II solution [2] to visualise the martensite. This etching results in a good contrast between martensite and austenite.

Tab. 1 Chemical composition in wt.-% of the X6CrNiTi18-10 specimens (Fe - balance)

C	Mn	P	S	Cr	Ni	Ti
0.05	1.08	0.039	0.019	17.55	9.86	0.39

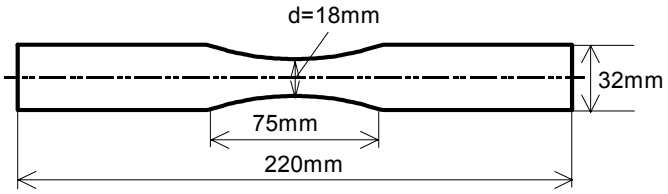
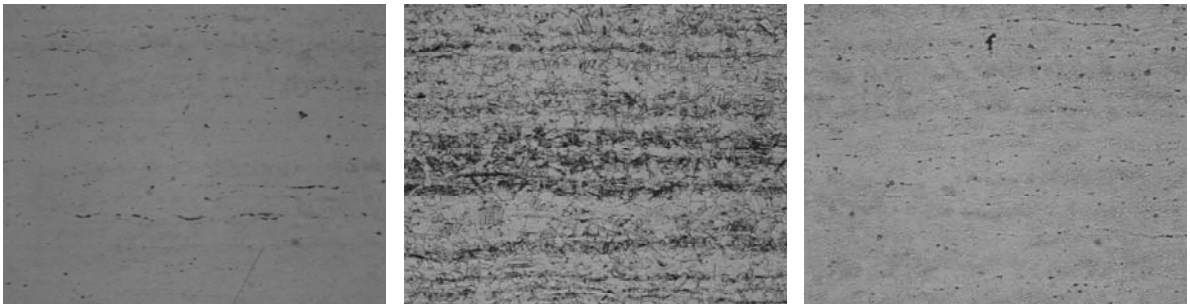


Fig. 1 Hour-glass specimens (ASTM E606)

3. Structure investigations

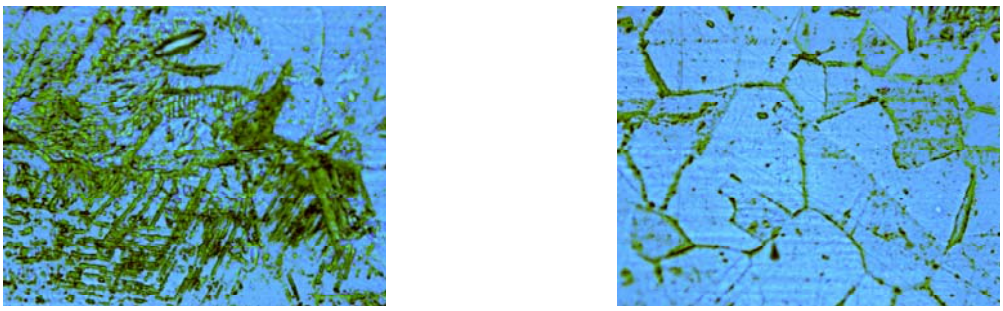
3.1. Metallography

For the metallographic investigations the sample 1.6 was used. Fig. 2 shows the microstructure at three axial positions. At positions close to the middle of the sample dark streaks were found. With increasing distances from the middle of the specimen the width of the streaks decreases down to zero. At positions far from the middle, the microstructure is homogeneous. The dark streak regions consists of martensite needles in an austenitic matrix (Fig. 3a). Outside these streaks only austenite grains can be found (Fig. 3b).



-30mm from the middle of the sample | middle of the sample | +30mm from the middle of the sample

Fig. 2 Microstructure of specimen 1.6 at different axial positions (eched with Beraha-II solution)



a) inside the streaks b) outside the streaks

Fig. 3 Microstructure in the middle of specimen 1.6 in- and outside the dark streaks

3.2. Neutron diffraction

The martensite content formed by phase changes was measured by means of neutron and X-ray diffraction. Austenite and martensite differ in their crystal structure. This makes it possible to determine the phase composition in the steel by neutron and X-ray diffraction experiments.

Neglecting textures, the volume fraction of martensite x in the two phase system (austenite and martensite) is given by [3]:

$$x = [(I_{\{h,k,l\}_{austenite}} / I_{(h,k,l)_{martensite}}) \cdot K_{1,2} + 1]^{-1} \quad (1)$$

$I_{\{h,k,l\}}$ is the intensity scattered at the lattice plane {h,k,l}. $K_{1,2}$ is a factor which considers the different structure type of martensite and austenite and the different angular positions of the reflexions. $K_{1,2}$ factors are tabulated for X-rays in [3] and can be calculated for neutrons [4]. A texture in the material can not be excluded. It is a real error source. Due to the one-dimensonal loading an fiber texture of the strain-induced martensite is to expect. However, for a homogeneous texture of the martensite the estimated martensite content differ from the real content by a constant factor. The relative information is not affected by this problem.
The neutron diffraction experiments were performed at the powder diffractometer DMC at the Swiss Spallation Neutron Source SINQ. With a neutron beam wave length of $\lambda = 0.38$ nm, a range of the scattering angle 2Θ of $68° \leq 2\Theta \leq 147°$ was analysed. The measurements on the vertically positioned LCF specimens were performed with a beam cross section of 40 mm (width) x 10 mm (height). The measuring position of these bulk measurements was in the middle of the LCF specimens (±5 mm in height). Due to the hour-glass sample shape the local strain amplitude depends on the axial sample position. It allows to analyse the strain dependence of the martensitic transformation by local measurements of the martensite content with a reduced beam height of 2 mm.
Results of martensite content x obtained by the bulk measurements are summarised in Tab. 2. Fig. 4 shows the local distributions of the martensite for four specimens. Three of them, sample 1.6, 2.3 and 2.5 have D = 1. The maxima of x are detected at the crack position also if the crack occurs not at the position with the smallest diameter. It seems that the crack formation results in an additional martensitic transformation. In the specimen 1.7 (without crack) the maximum of the martensite content was found at the smallest cross section. The martensite distribution in axial direction is non-symmetric for this specimen.

Tab. 2 Martensite content obtained by neutron diffraction

Sample No.	Cycle number	Usage factor D	Crack position	Martensit (vol.-%)
1.2	0	0	-	< 0.50
2.4	0	0	-	< 0.50
1.8	11200	0.4	-	< 0.50
1.4	15850	0.6	-	0.61
2.2	15850	0.6	-	0.54
1.3	22400	0.8	-	0.95
1.7	22400	0.8	-	0.93
2.5	26000	1.0	5 mm away from the middle	1.49
2.3	32000	1.0	in the middle	1.49
1.6	63200	1.0	in the middle	3.13

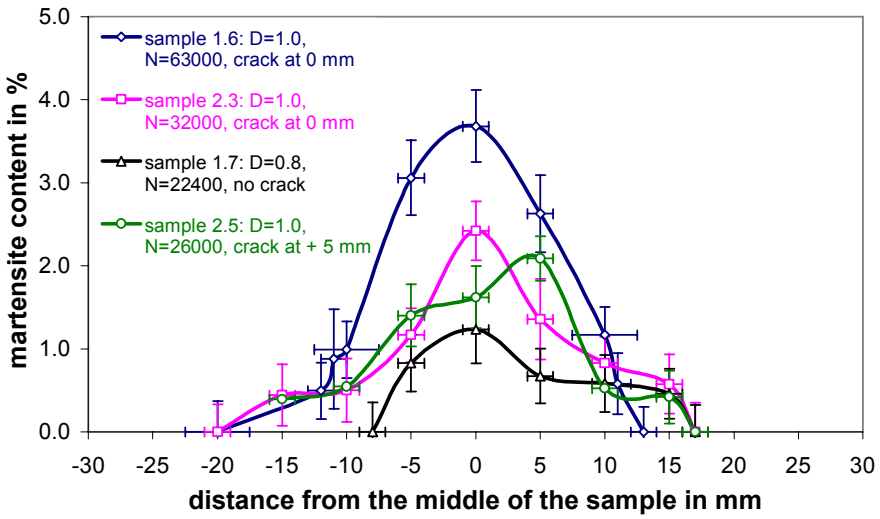


Fig. 4 Axial distribution of the martensite content for specimens 1.6, 1.7, 2.3 and 2.5

According to the Coffin-Manson relation the parameter A shall be introduced with

$$A = \sqrt{N} \cdot \varepsilon_{a,p} \tag{1}$$

N is the cycle number and $\varepsilon_{a,p}$ the half of the plastic strain amplitude. A is a measure for the accumulated plastic strain. In Fig. 5, x is plotted as a function of A. The values obtained at positions where a crack was observed are excluded. Below a threshold value no martensite was detectable by neutron diffraction (detection limit is about 0.5 vol.-%). For values higher than the threshold, a linear dependence of the martensite content on the accumulated strain amplitude was found.

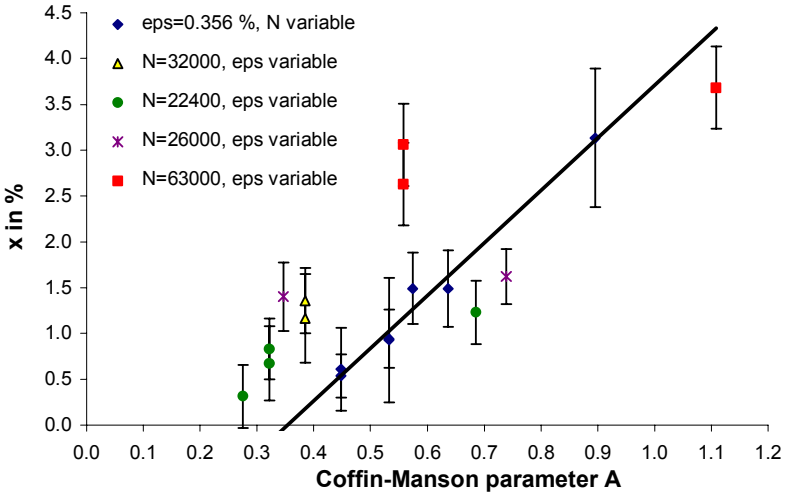


Fig. 5 Dependence of martensite content x on the accumulated plastic strain

3.3. X-ray diffraction (XRD)

Due to the high intensity X-ray diffraction experiments using synchrotron light sources enable to analyse martensite distribution in two dimensions with higher local resolution than neutron diffraction in shorter measurement periods. They give additional information on the radial distribution of martensite near the cut surface. The X-ray diffraction experiments were performed at the ROBL beamline at ESRF Grenoble (France) [6]. In order to use the $K_{1,2}$ values from [3], the wavelength of the Mo-Kα radiation (λ = 0.07107 nm) was applied. The investigated specimen 1.6 was cut into two halves parallel to the sample axis. A mapping of the axial and radial martensite distribution was obtained by scanning the specimen through the fixed beam. With the applied wave length and the beam cross section of 0.2 mm x 0.5 mm the gauge volume was about 1 mm (axial) x 0.5 mm (radial) x 0.005 mm (in depth).

Fig. 6 shows the axial and radial mapping of the martensite content of specimen 1.6 determined from the X-ray diffraction data. In agreement with the ND measurements, in the axial direction, the martensite is found at the smallest cross section of the specimen according to the concentration of the plastic strain. In the radial direction, the martensite content is concentrated near the surface (y = -6 and 7 mm) and, as a broad area, in the centre of the specimen (x, y = 0 mm). The highest portion of martensite was found at the crack tip position. At the opposite site of the specimen the specimen the martensite content is significant lower. It confirms that the crack formation and growth is accompanied with an additional martensitic transformation.

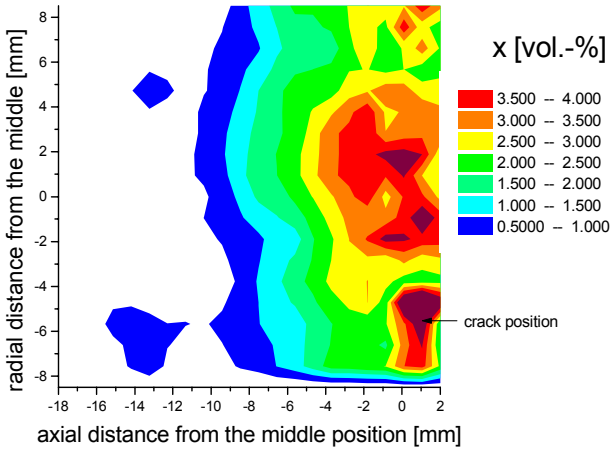


Fig. 6 Mapping of the radial and axial distribution of the martensite content x of specimen 1.6

4. Testing for LCF degradation by means of magnetic NDT methods

4.1 Measurements of magnetic stray field strength

Due to the ferromagnetism of martensite it is possible to apply a passive magnetic technique. After magnetising the specimens, the remanent field strength can be measured. The magnetisation of the specimens was carried out in a field with a strength of about 11 kA/m. Afterwards all specimens were examined using high sensitive fluxgate sensors. Measurements of the axial and normal components of the magnetic stray field were performed in a distance of 20 mm from the bar axis. The fluxgate sensor was sensitive enough to detect martensitic areas.

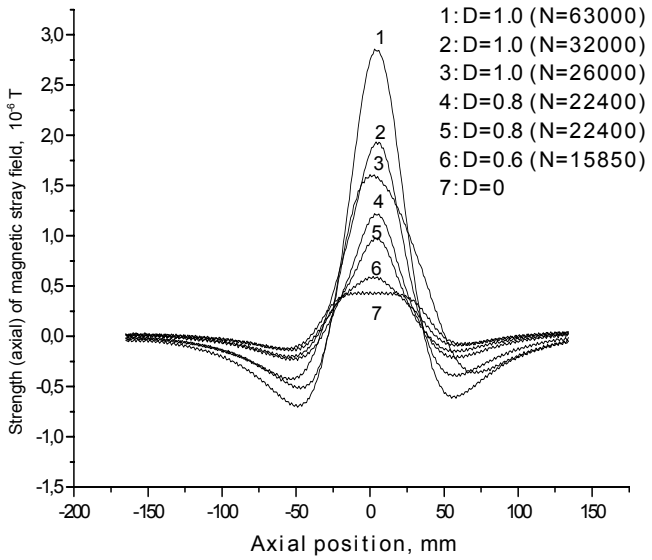


Fig. 7 Stray field measurements (fluxgate output) at LCF specimens of different usage factors, cycle numbers

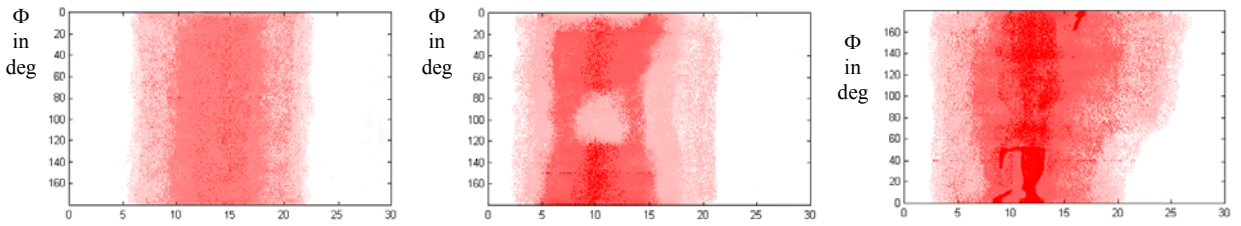
In Fig. 7 the fluxgate output (axial component) is plotted as a function of the axial scanning position. This output shows a pronounced positive peak when the sensor is directly over the position of the smallest cross section of the LCF samples. In the case of measurements on samples with cracks (D = 1), the amplitude of field strength depends on the cycle number. For the pre-crack stages the amplitude of the fluxgate output increased with the usage factor or with the corresponding cycle numbers. The LCF damage in the specimens was detected down to the usage factor of D = 0.6. At lower D the fluxgate output does not differ significantly.

4.2 Measurements by means of eddy current techniques

Eddy current techniques seem to be very promising for detecting LCF degradation. If the eddy current field is disturbed locally by changes of permeability, the eddy current signal is changed. The induced voltage amplitude with reference to a defined phase angle of the receiving coil was recorded. The manipulator system applied was able to follow the hour-glass shape of the specimens in a distance between sensor and surface of 1 mm. For martensite visualisation a frequency of 50 kHz was used which provides a reasonable balance between high local resolution and depth of the eddy current field in the steel. The lower and upper bound of 0.5 and 3.15 vol.-% martensite content define the adjustment of the eddy current sensitivity.

For eddy current measurements, the end pieces of the LCF specimens were cut off and only the middle sections were used. Some examples of eddy current measurements performed at the circumferencial surface are plotted in Fig. 8. The axial specimen direction corresponds to the abscissa, the circumferential specimen directions (Φ-angle) correspond to the ordinate. Plots are shown for specimens with different usage factor (1.4, 1.7 and 2.3 with D = 0.6, 0.8 and 1.0, respectively). The martensite content of 0.61 vol.-% for specimen 1.4 was clearly detected. The martensite is homogeneously distributed in the circumferential direction. The

plot shows the beginning of the martensite formation during LCF loading. In the following damage stages D = 0.8 and D = 1.0, the martensitic pattern is the darker the more usage factor increases. For specimen 1.7, the martensite is not as homogeneously distributed as for specimen 1.4. It agrees with the results of neutron scattering investigations. It is possible that the axial loading was accompained by a small amount of bending.



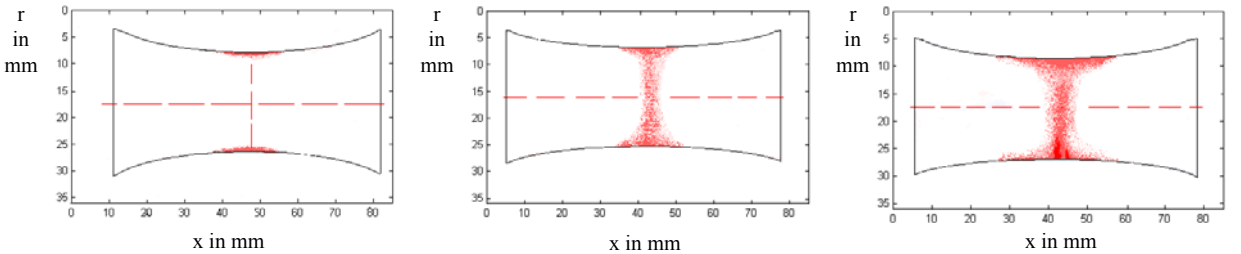
sample 1.4 (D=0.6, x_M=0.61 vol.-%) sample 1.7 (D=0.8, x_M=0.93 vol.-%) sample 2.3 (D=1.0, x_M=1.49 vol.-%)

Fig. 8 Eddy current measurements in dependence on the angle Φ and on the axial pisition (x) on the circumferencial surface of LCF specimens

For specimen 2.3, loaded up to crack initiation, a single large crack was detected at the position of the smallest cross section. Furthermore, some local areas with a very high martensite concentration were found. These are probably new sources for macroscopic cracks. The martensite is homogeneously distributed. At the crack position an additional formation of martensite was observed.

Additionally, the specimens were cut lengthwise into two halves. Thus it is possible to determine the martensite distribution also in the radial specimen direction and obtain information about the progress of the martensite formation. In Fig. 9, the eddy current signal amplitudes at the axial cross section surface are plotted. The sensor output for specimen 1.4 shows, that the formation of martensite is limited to the surface at the position of the smallest cross section. No martensite was detected in bulk.

For further damage progression (specimen 1.7), the martensite tends to spread in depth. The distribution of martensite in the axial direction is wider at the surface than in the bulk. It seems that macroscopic crack initiation affects stress relaxation around this location. This results in a decrease of the martensite spreading in this area which is shown for specimen 2.3. The shape of the martensitic pattern is broader at the opposite side of the crack.



sample 1.4 (D=0.6, x_M=0.61 vol.-%) sample 1.7 (D=0.8, x_M=0.93 vol.-%) sample 2.3 (D=1.0, x_M=1.49 vol.-%)

Fig. 9 Eddy current measurements in dependence on the radial (r) and axial (x) position on axial cross section of LCF specimens

5 Conclusions

All applied methods (neutron and X-ray diffraction, magnetic stray field measurements with SQUID and fluxgate sensors, eddy current measurement) allowed the detection of martensite. While the amount of martensite is quantified with the diffraction methods, the magnetic techniques yield only relative results; that means, they have to be calibrated somehow, i.e. with results from neutron diffraction experiments.

It was shown that the content of martensite depends on the accumulated plastic strain and therefore the on usage factor. The existence of a threshold for the accumulated strain to form deformation-induced martensite was demonstrated. This threshold is useful when examining industrial components under service conditions. The dependence of the threshold on other conditions of loading and temperature should be investigated in detail.

For our testing conditions the eddy current technique was able to detect LCF damage down to $D = 0.6$, the stray field measurements down to $D = 0.8$. No significant differences of measuring signals for both techniques were found for $D < 0.6$, which corresponds to the results obtained by neutron diffraction experiments.

6 Acknowledgments

This work was supported by the Swiss Federal Nuclear Safety Inspectorate, HSK.

References

[1] "Experience with thermal fatigue in LWR piping caused by thermal mixing and stratification.", Paris: OECD Nuclear Energy Agency, 1998. OECD NEA CSNI R(98)8

[2] E.Weck, E.Leistner: "Metallographische Anleitung zum Farbätzen nach dem Tauchverfahren, Band2: Farbätzung nach Beraha und ihre Anwendungen.", Deutscher Verlag für Schweisstechnik, Düsseldorf, 1983

[3] G.Fanninger, U.Hartmann: Härterei Technische Mitteilungen HTM 27, (1972), 233

[4] G.E.Bacon: "Neutron Diffraction", Oxford: Clarendon Press, 1975.

[5] http://www1.psi.ch/www_sinq_hn/SINQ/instr/ DMC.html

[6] W.Matz et al.: J. Synchr. Rad. 6, 1999, p. 1076